This is the accepted manuscript made available via CHORUS. The article has been published as:

Quantum paramagnetism in a non-Kramers rare-earth oxide: Monoclinic math xmlns="http://www.w3.org/1998/Math/MathML">mrow>msub>mi>Pr/mi>mn>2/mn>/msub>msub>mi>Ti/mi>mn>2/mn>/msub>msub>mi mathvariant="normal">O/mi>mn>7/mn>/msub>/mrow>/math>

Huiyuan Man, Alireza Ghasemi, Moein Adnani, Maxime A. Siegler, Elaf A. Anber, Yufan Li, Chia-Ling Chien, Mitra L. Taheri, Ching-Wu Chu, Collin L. Broholm, and Seyed M. Koohpayeh

Phys. Rev. Materials **7**, 063401 — Published 16 June 2023

DOI: 10.1103/PhysRevMaterials.7.063401

Quantum paramagnetism in a non-Kramers rare-earth oxide: Monoclinic $Pr_2Ti_2O_7$

Huiyuan Man,[1] Alireza Ghasemi,[1] Moein Adnani,[2] Maxime A. Siegler,[3] Elaf A. Anber,[4] Yufan Li,[5] Chia-Ling Chien,[5,6,7] Mitra L. Taheri,[4] Ching-Wu Chu,[2,8] Collin L. Broholm,[1,4] and Seyed M. Koohpayeh[1,4,9,*]

[1] *Institute for Quantum Matter and Department of Physics and Astronomy, The Johns Hopkins University, Baltimore, MD 21218, USA*
[2] *Texas Center for Superconductivity and Department of Physics, University of Houston, Houston, TX 77204, USA*
[3] *Department of Chemistry, The Johns Hopkins University, Baltimore, MD 21218, USA*
[4] *Department of Materials Science and Engineering, The Johns Hopkins University, Baltimore, MD 21218, USA*
[5] *Department of Physics and Astronomy, The Johns Hopkins University, Baltimore, MD 21218, USA*
[6] *Institute of Physics, Academia Sinica, Taipei 11519, Taiwan*
[7] *Department of Physics, National Taiwan University, Taipei 10617, Taiwan*
[8] *Lawrence Berkeley National Laboratory, Berkeley, CA 94720, USA*
[9] *Ralph O'Connor Sustainable Energy Institute, Johns Hopkins University, Baltimore, MD 21218, USA*

(Dated: May 22, 2023)

Little is so far known about the magnetism of the $A_2B_2O_7$ monoclinic layered perovskites that replace the spin-ice supporting pyrochlore structure for $r_A/r_B > 1.78$. We show that high quality monoclinic $Pr_2Ti_2O_7$ single crystals with a three-dimensional network of non-Kramers Pr^{3+} ions that interact through edge-sharing super-exchange interactions, form a singlet ground state quantum paramagnet that does not undergo any magnetic phase transitions down to at least 1.8 K. The chemical phase stability, structure, and magnetic properties of the layered perovskite $Pr_2Ti_2O_7$ were investigated using x-ray diffraction, transmission electron microscopy, and magnetization measurements. Synthesis of polycrystalline samples with the nominal compositions of $Pr_2Ti_{2+x}O_7$ ($-0.16 \leq x \leq 0.16$) showed that deviations from the $Pr_2Ti_2O_7$ stoichiometry lead to secondary phases of related, structures including the perovskite phase $Pr_{2/3}TiO_3$ and the orthorhombic phases $Pr_4Ti_9O_{24}$ and Pr_2TiO_5. No indications of site disordering (stuffing and anti-stuffing) or vacancy defects were observed in the $Pr_2Ti_2O_7$ majority phase. A procedure for growth of high-structural-quality, stoichiometric single crystals of $Pr_2Ti_2O_7$ by the traveling solvent floating zone (TSFZ) method is reported. Thermo-magnetic measurements of single-crystalline $Pr_2Ti_2O_7$ reveal an isolated singlet ground state that we associate with the low symmetry crystal electric field environments that split the $2J + 1 = 9$-fold degenerate spin-orbital multiplets of the four differently coordinated Pr^{3+} ions into 36 isolated singlets resulting in an anisotropic temperature independent van-Vleck susceptibility at low T. A small isotropic Curie term is associated with 0.96(2)% non-interacting Pr^{4+} impurities.

I. INTRODUCTION

The ternary oxides of the family $A_2B_2O_7$, predominantly with the face-centered cubic pyrochlore lattice in which A^{3+} is a trivalent cation and B^{4+} is a transition metal, have been extensively studied due to a wide variety of interesting physical properties[1]. These include the anomalous Hall effect in $Nd_2Mo_2O_7$[2], giant magnetoresistance in $Tl_2Mn_2O_7$[3–5], superconductivity in $Cd_2Re_2O_7$[6], a phase transition from a paramagnetic metal to an antiferromagnetic insulator in $Eu_2Ir_2O_7$[7], and classic spin ice in $Dy_2Ti_2O_7$ and $Ho_2Ti_2O_7$[8–11]. Pyrochlore magnets are also promising systems for realizing 3-dimensional quantum spin liquids[11,12] and other exotic states of matter[13–25].

Among the extensively studied rare-earth titanates ($RE_2Ti_2O_7$), those which adopt the layered perovskite monoclinic structure have been relatively less explored. The formation and stability of this layered structure depends on the ratio r_A/r_B between the radii of the A^{3+} and B^{4+} cations (here Pr^{3+} and Ti^{4+}). For $r_A/r_B > 1.78$, which occurs for La, Ce, Pr, Nd, the low-symmetry layered-perovskite monoclinic structure (space group $P2_1$) is preferred, while in the range $1.48 \leq r_A/r_B \leq 1.78$ (from Sm to Lu and Y) the titanates form the cubic pyrochlore structure (space group $Fd\overline{3}m$)[26,27].

The monoclinic structure is described by four (001) layers ($n = 4$) of corner-sharing TiO_6 octahedra that form a perovskite-like slab separated by two (001) layers of RE-site cations (Fig. 1). Praseodymium occupies four 2a Wyckoff sites that fall in two groups. Located in the perovskite slab within interstices defined by the TiO_6 octahedra, Pr1 and Pr4 are 12-fold and 7-fold coordinated by oxygen, respectively. Pr2 and Pr3 with oxygen coordination number 10, bracket the perovskite slabs[28]. Since these four Pr sites carry the low C_2^2 point group symmetry, the $J = 4$ spin-orbital multiplet of Pr^{3+} must be split into 9 non-magnetic singlet levels. In addition, as the four sites are different, a total of 4×36 singlet crystal field levels should be anticipated. If the energy scale for interactions is less than the splitting between the singlet ground state and the first excited singlet, then we can expect $Pr_2Ti_2O_7$ to form a paramagnetic band insulator, which although magnetizable, should not in gen-

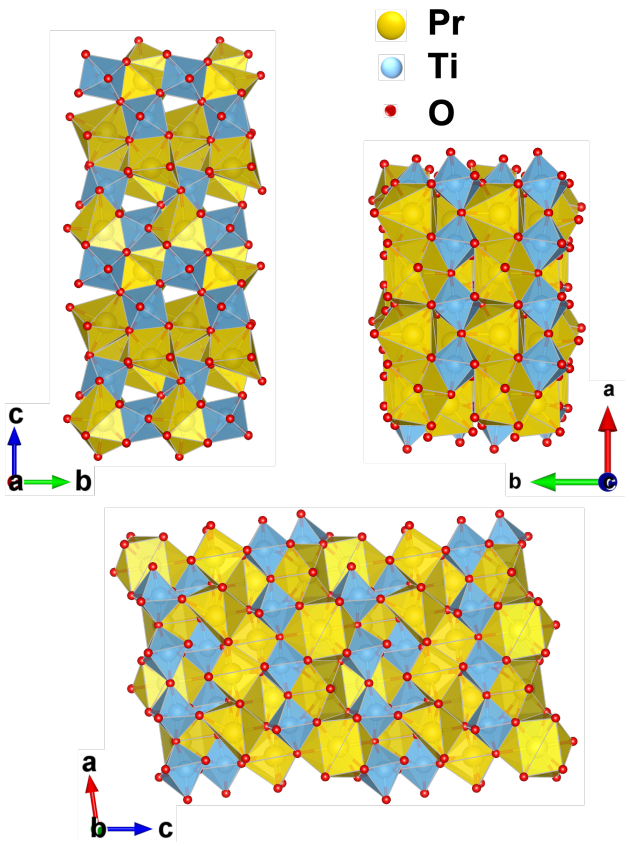


FIG. 1. Layered-perovskite monoclinic crystal structure of $Pr_2Ti_2O_7$. The structure consists of two-dimensional infinite perovskite slabs (four layers of corner-sharing TiO_6 octahedra) that are separated from each other by two praseodymium-rich layers. There are four formula units per monoclinic unit cell.

eral be expected to undergo a magnetic phase transition. It should however, be possible to drive the material to quantum criticality and an ordered state through the application of pressure or field at low temperatures.

The monoclinic layered perovskite titanates were previously studied for their interesting ferroelectric[29–36], piezoelectric[30], nonlinear optical[37], photocatalytic[38,39], and dielectric[29,39,40] properties, as well as their high ferroelectric Curie temperature[33–35]. Monoclinic $Pr_2Ti_2O_7$, in particular, was grown and studied as powder through solid-state reaction[27], nanoparticles through the sol-gel method[29] or the modified self-propagated high-temperature synthesis (SHS) method[40], and as epitaxial thin films grown by pulsed laser deposition (PLD)[30]. Single-crystal synthesis was also reported[37,41]. The powder samples of $Pr_2Ti_2O_7$ showed a monoclinic structure in the non-centrosymmetric $P2_1$ space group and were investigated by X-ray diffraction and Raman spectroscopy[27,31,42]. The electronic structure of $Pr_2Ti_2O_7$ has been studied with X-ray photoelectron spectroscopy (XPS)[32,38], and the optical properties were investigated by first-principles density functional theory calculations[39]. The photocatalytic activity of $RE_2Ti_2O_7$ (RE = La, Pr, Nd) is highly dependent on their electronic band structure[38]. Ferroelectric measurements showed a Curie temperature beyond 1555(5) °C[33], while similar properties were observed for monoclinic $La_2Ti_2O_7$ and $Nd_2Ti_2O_7$ with Curie temperatures of 1461(5) °C[34,35] and 1482(5) °C[35], respectively. The temperature-dependent Raman spectroscopy is very different for the pyrochlore "dynamic spin-ice" compound $Pr_2Sn_2O_7$ and its non-pyrochlore (monoclinic) counterpart $Pr_2Ti_2O_7$[41].

To our knowledge there has been no comprehensive study of the phases, structures and disorders associated with the compositional deviations from the stoichiometric $Pr_2Ti_2O_7$. As we shall see this reveals a distinct contrast in chemical solubility compared to pyrochlore titanates. An investigation of the low-symmetry lattice structure's effect on the low temperature magnetic properties of $Pr_2Ti_2O_7$ is also lacking. In this work, we report a systematic investigation of the phase and structural stability of $Pr_2Ti_2O_7$ based on synthesis of polycrystalline powders and single crystals. A process to develop a stoichiometric high-quality $Pr_2Ti_2O_7$ single crystal by the traveling solvent floating zone (TSFZ) technique is reported for the first time. In order to understand the role which the lattice structure plays in determining the magnetic properties, single crystalline $Pr_2Ti_2O_7$ is characterized through magnetization measurements versus temperature, field, and crystalline directions. Our study shows there is no magnetic ordering and the non-Kramers Pr^{3+} ions form singlet ground states with an energy gap to excited states. The presence of a three dimensional network of edge-sharing praseodymium oxide polyhedra suggest that it may be possible to induce a quantum phase transition to an ordered state through the application of pressure, strain, or high magnetic fields.

II. EXPERIMENTAL DETAILS

A. Synthesis of powders

Powder samples of praseodymium titanates with nominal compositions $Pr_2Ti_{2+x}O_7$, $-0.16 \leq x \leq 0.16$ were synthesized by the solid-state reaction method. The Pr_6O_{11} (99.99% Alfa Aesar) and TiO_2 (99.99% Alfa Aesar) starting materials were dried at 1050 °C for 10 hours. Pr_6O_{11} powder was reduced to Pr_2O_3 in a hydrogen atmosphere. The resulting powders were then weighed and the appropriate ratio was mixed, thoroughly ground, and heated to 1300 °C in air for 10 hours. The process of mixing, grinding, and heating was repeated four times.

B. Single-crystal growth

Crystal growth of praseodymium titanates was carried out using the floating-zone melting technique[43,44]

in a four-mirror image furnace equipped with four 1 kW halogen lamps (Crystal Systems, Inc., FZ-T-4000-H-VII-VPO-PC). Powder samples of stoichiometric $Pr_2Ti_2O_7$ were first pressed into rods typically 5 mm in diameter and 8 cm in length and sintered in air at 1300 °C for 10 hours. The feed rod and the seed rod were mounted on the upper and lower shafts of the furnace, respectively, with the mirror stage moving upward during the growth process. The rotation speeds of the upper and lower shafts were 3 rpm and 6 rpm, respectively, during growth.

C. Characterization

The resulting phases, crystal structures, and lattice parameters were determined using powder x-ray diffraction (XRD) at room temperature. Data were acquired for 4 hours covering a scattering angle range $5° < 2\theta < 100°$ on a Bruker D8 focus diffractometer with monochromatic Cu K_α radiation and a LynxEye strip detector. Standard Si (silicon) powder was added as a reference into the samples. Rietveld refinement of the XRD patterns was carried out using TOPAS software (Bruker AXS).

All reflection intensities of single-crystalline $Pr_2Ti_2O_7$ were measured at 213(2) K using a SuperNova diffractometer (equipped with an Atlas detector) with Mo K_α radiation ($\lambda = 0.71073$ Å) under the program CrysAlisPro (Version CrysAlisPro 1.171.39.29c, Rigaku OD, 2017). The same program was used to refine the cell dimensions and for data reduction. The structure was solved with the program SHELXS-2018/3 and was refined against the squared structure factor with SHELXL-2018/3[45]. Empirical absorption correction using spherical harmonics was applied through CrysAlisPro. The sample temperature during data acquisition was controlled using a Cryojet system (manufactured by Oxford Instruments).

The single crystals were oriented using a tungsten anode back-reflection x-ray Laue diffractometer with a 1 mm diameter x-ray beam spot. A single crystal oriented with (100), (010), and (001) planes was cut using a diamond wire saw to the dimension of $1.28 \times 1.58 \times 2.47$ mm^3 respectively for a mass of 29.8 mg. For transmission electron microscopy (TEM), samples were prepared by crushing as-grown crystals in ethanol and placing a single drop of the solvent on a TEM carbon grid. We used a JEOL 2100 field emission TEM equipped with a high-resolution pole piece. Temperature-dependent susceptibility and isothermal magnetization measurements were performed using a Quantum Design SQUID (superconducting quantum interference device) magnetometer on the single crystal mentioned above in three different orientations and on a stoichiometric polycrystalline sample.

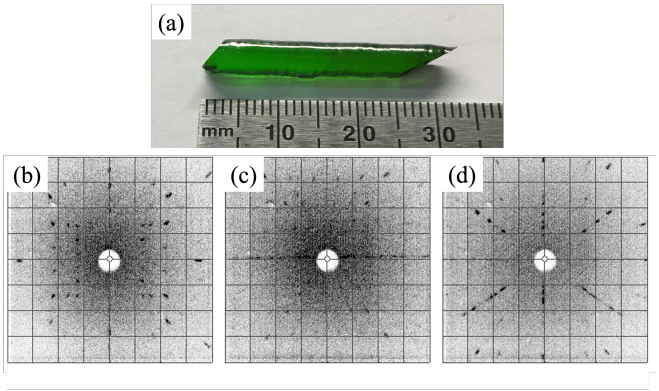


FIG. 2. (a) Image of the $Pr_2Ti_2O_7$ single-crystal grown by the traveling solvent floating-zone (TSFZ) technique. (b-d) Laue back-reflection x-ray diffraction patterns taken with the beam incident normal to the (100), (010) and (001) planes, respectively.

III. EXPERIMENTAL RESULTS

A. Polycrystalline $Pr_2Ti_2O_7$

Contrary to the high temperature dynamic melt/liquid-zoning crystal growth processes, solid-state powder synthesis at lower temperatures is a highly controllable process to explore both stoichiometric $Pr_2Ti_2O_7$ and neighboring off-stoichiometric phase(s)/structures. Detailed in the supplementary material[46] (see also references[47–67] therein), our study of the effect of variations in the net reagent composition in $Pr_2Ti_{2+x}O_7$ for $(-0.16 \leq x \leq 0.16)$ shows the monoclinic phase forms as a stoichiometric compound mixed with secondary phases to accommodate the reagent composition. This sets $Pr_2Ti_2O_7$ apart from the cubic rare earth pyrochlores, which can deviate considerably from the ideal 2:2:7 stoichiometry. The stability of $Pr_2Ti_2O_7$ as a stoichiometric solid, facilitates the process of growing high quality stoichiometric single crystals.

B. Single crystal of $Pr_2Ti_2O_7$

Though high-temperature phase instabilities and incongruent melting were encountered during the float-zone (FZ) melting process, crystal growths of $Pr_2Ti_2O_7$ were successfully performed by the traveling solvent floating zone technique (TSFZ) under 1 bar static UHP argon. The growth was stable during the entire process at the consistent lamp power of 56.5%, and no vaporization was observed. A typical transparent and green $Pr_2Ti_2O_7$ crystal together with the Laue patterns along the main crystallographic planes are shown in Fig. 2. x-ray Laue patterns taken at regular intervals along the lengths and cross sections of the crystals indicated high crystalline

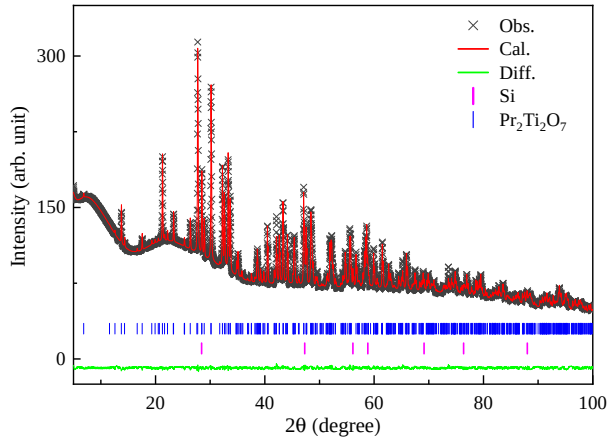


FIG. 3. Rietveld refinement of XRD pattern taken from powder formed by crushing a $Pr_2Ti_2O_7$ single-crystal. The collected pattern is in black, the simulated pattern is in red, and the difference is in green. Locations of Bragg reflections for Si and $Pr_2Ti_2O_7$ are marked as pink and blue vertical bars, respectively. The background arises from the quartz sample plate.

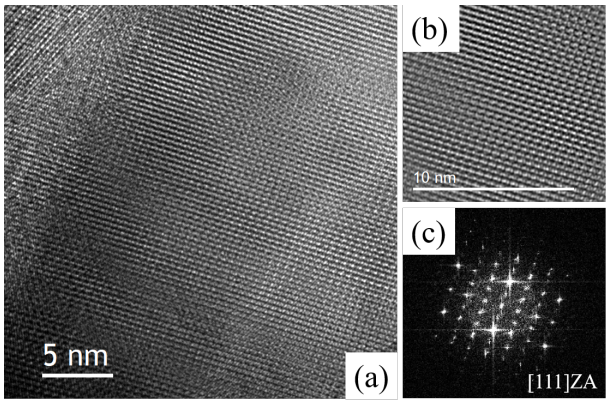


FIG. 4. (a) High-resolution transmission electron microscopy (HRTEM) image of $Pr_2Ti_2O_7$ crystal. (b) The corresponding inverse fast Fourier transform (IFFT) image. (c) Fast Fourier transformation (FFT) image, showing the reflection with beam incident along the [111] direction.

quality with no detectable variation of orientation and no evidence of spot splitting or distortion. The crystal showed an easy cleavage along the (001) plane.

The Rietveld refinement of the XRD pattern (Fig. 3) taken from the crushed crystal at room temperature confirms that the crystal is single phase, the structure is monoclinic with space group $P2_1$, and the lattice constants were measured to be $a = 7.7116$ Å, $b = 5.4867$ Å, $c = 13.0072$ Å, and $\beta = 98.5563°$, similar to the stoichiometric powder sample.

The crystal data and structure refinement for $Pr_2Ti_2O_7$ measured at 213(2) K is shown in Table S2. The occupancy factors for PrX and TiX (X = 1, 2, 3, 4) were all refined freely in Table S3, and their final values are: Pr1 0.970(5), Pr2 0.969(5), Pr3 0.959(5), Pr4 0.961(5), Ti1 0.966(6), Ti2 0.964(6), Ti3 0.963(6), and Ti4 0.955(6). The occupancy factors for all O atoms refine to 1 within their standard uncertainties, and were all constrained to be 1 in the final refinement. The absolute configuration has been established by anomalous dispersion effects in diffraction measurements on the crystal, and the Flack and Hooft parameters refine to -0.024(11) and -0.026(9), respectively.

Single crystals of $Pr_2Ti_2O_7$ were further examined by high-resolution transmission electron microscopy (HRTEM) from the [111] zone axis, indicating a crystal of high structural quality (Fig. 4).

C. Magnetization measurements

The high quality $Pr_2Ti_2O_7$ single crystals described in the previous sections enabled us to explore the anisotropic magnetism of interacting non-Kramers rare earth ions occupying four distinct low symmetry sites. Prior experiments characterizing the physical properties of $Pr_2Ti_2O_7$ are quite limited. Room temperature ferromagnetism was reported for polycrystalline $Pr_2Ti_2O_7$ nanoparticles grown through the sol-gel method. This effect is however, unrelated to the rare earth magnetism and appears to be connected with oxygen vacancies at the surfaces of nanoparticles[29]. A Raman study on a single crystal of $Pr_2Ti_2O_7$ synthesized by the float-zone method revealed structural stability up to 18 GPa and a complex spectrum as the low symmetry monoclinic space group leads to 129 Raman active optical phonons[41,69].

We measured the temperature-dependent magnetic susceptibility for both the single- and poly-crystalline $Pr_2Ti_2O_7$ samples. Fig. 5(a) shows $M(T)/B$ as a function of temperature for applied fields normal to the (001) plane ranging from 100 Oe to 70 kOe. No anomalies or hysteresis is observed down to $T = 1.8$ K. This indicates $Pr_2Ti_2O_7$ has no magnetic phase transition in this temperature and field range. The field dependence of $M(T)/B$ at low T for $B < 15$ kOe indicates the presence of paramagnetic impurities. We use measurements of $M(T)$ at $B = 1$ kOe to report the magnetic susceptibility $\chi(T) \equiv M(T)/B$ versus temperature and field direction in Fig. 5(b). As should be anticipated for the non-Kramers ion Pr^{3+} in a monoclinic structure, there is considerable single ion crystal electric field driven anisotropy with more than a factor 2 difference in low T susceptibility for the easy (100) versus the hard (001) directions. No field direction has indications of a magnetic phase transition. The inset shows the ratio of the single crystal to powder sample magnetic susceptibility versus T, which provides a dimensionless measure of the magnetic anisotropy. The anisotropy is reduced at higher T which indicates population of excited crystal field levels in that temperature range. An upturn in $\chi(T)$ is apparent at the lowest temperatures for both the single-crystal and polycrystalline sample. As detailed later, we associate

TABLE I: The fitting parameters from analysis of the $T-$dependent susceptibility of monoclinic $Pr_2Ti_2O_7$ for various directions (α) of a single crystal, the average of parameters for those three directions, and obtained for a polycrystalline sample.

Field direction (α)	$C_0^{\alpha\alpha}$ ($\frac{\text{emu K}}{\text{Oe mole Pr}}$)	$C_1^{\alpha\alpha}$ ($\frac{\text{emu K}}{\text{Oe mole Pr}}$)	Δ_1^{α} (meV)	$C_2^{\alpha\alpha}$ ($\frac{\text{emu K}}{\text{Oe mole Pr}}$)	Δ_2^{α} (meV)
$\alpha = (100)$	0.0054(2)	0.50(2)	3.93(7)	1.03(2)	9.2(1)
$\alpha = (010)$	0.0046(1)	0.789(3)	6.99(2)	0.84(1)	50(1)
$\alpha = (001)$	0.0050(2)	0.324(3)	4.72(4)	0.805(5)	28.4(4)
average	0.0050(2)	0.54(2)	5.2(1)	0.89(2)	29.2(4)
powder sample	0.0086(3)	0.711(9)	5.55(5)	0.918(8)	28.3(7)

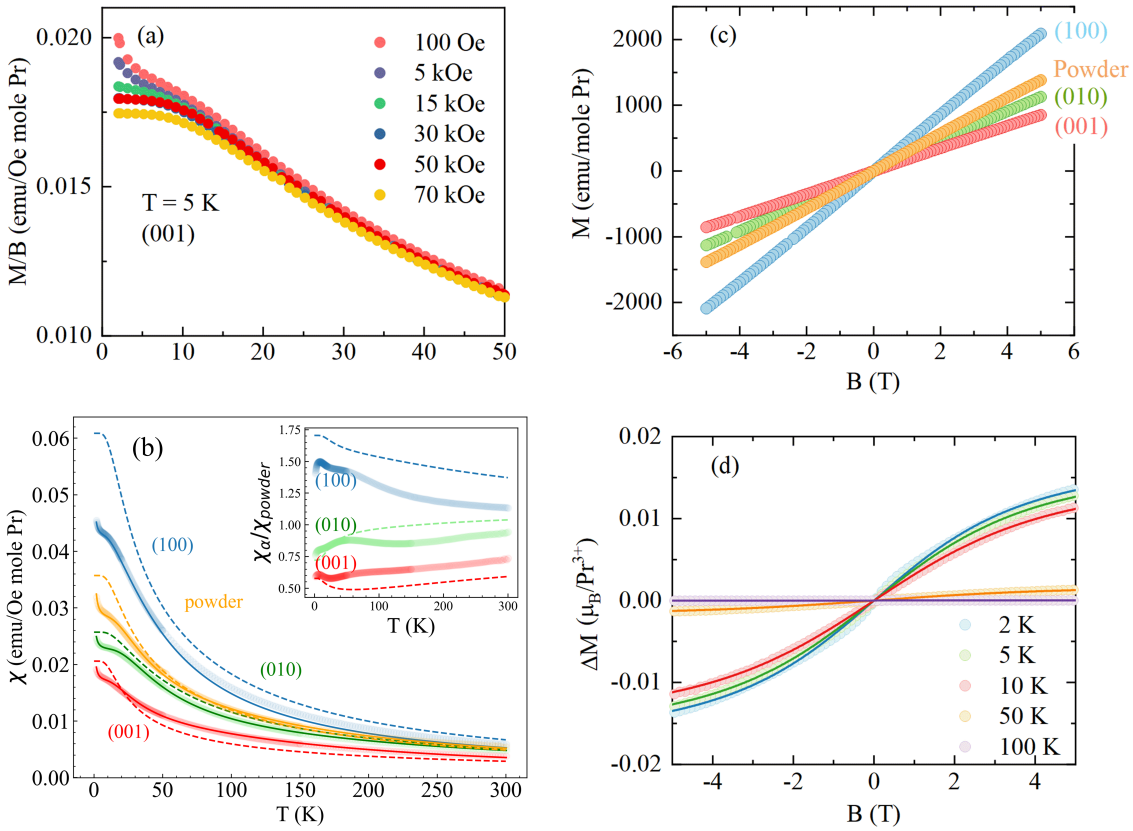


FIG. 5. Magnetization data for single crystal and polycrystalline samples of monoclinic $Pr_2Ti_2O_7$. (a) Temperature-dependent "susceptibility" $M(B,T)/B$ for fields normal to the (001) plane under ZFC condition with multiple measurement fields. Demagnetization corrections are negligible. (b) Susceptibility inferred from magnetization measurements in a field of 1 kOe while warming from 1.8 K to 300 K. The solid lines show best fits to Eq. (1) with the parameters listed in Table (I). Dashed lines represent the susceptibility calculated from Crystal Field calculation[68] using point charge model. The inset shows the ratio of the single crystal to powder sample magnetic susceptibility versus T. (c) Isothermal magnetization measured at 5 K for the three directions of a single crystal and for a polycrystalline sample of $Pr_2Ti_2O_7$. (d) Non-linear part of the isothermal magnetization $\Delta M(B,T)$ for fields normal to the (001) plane at various temperatures. The linear part determined by fitting data for $|B| > 6.5$ T in (c) was subtracted. The fits to $\Delta M(B,T)$ are based on Eq. (3) and yield an impurity concentration of $f = 0.96(2)\%$ with an average saturation moment of $\mu_{sat} = 2.00(3)\ \mu_B$.

this "Curie tail" with paramagnetic Pr^{4+} impurities.

IV. ANALYSIS AND DISCUSSION

A. Phenomenological crystal field level scheme

With the $J = 4$ non-Kramers Pr^{3+} ion in four different sites with C_2^2 symmetry there should be 36 crystal field levels in $Pr_2Ti_2O_7$. Neutron and/or Raman scat-

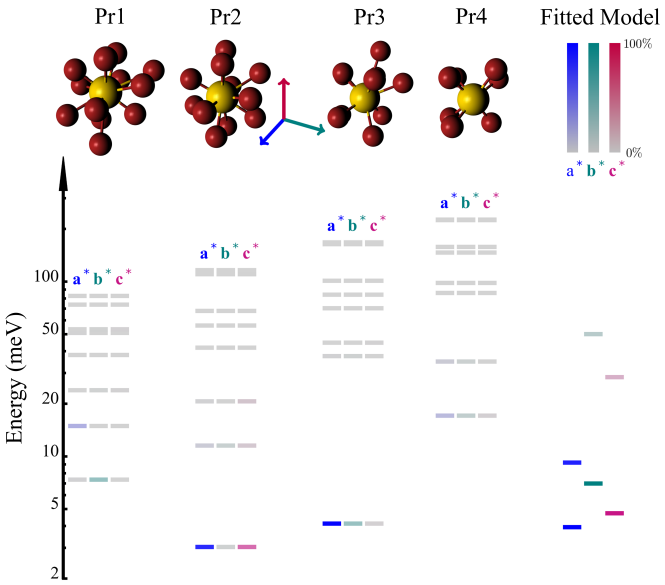


FIG. 6. Crystal field level scheme calculated for each of the four distinct Pr^{3+} Wyckoff sites in $Pr_2Ti_2O_7$ with a comparison to the site averaged level scheme inferred from susceptibility data (far right). The strength of each crystal field level's van Vleck contribution to the magnetic susceptibility in the low T limit is indicated by the color of that level refering to the upper right color bars with cyan, green, and red associated with the three directions respectively. $\mathbf{a}^*$, $\mathbf{b}^*$, and $\mathbf{c}^*$ are the directions normal to the (100), (010), and (001) planes. Gray levels do not contribute to the magnetic susceptibility at low T for the indicated field direction. The coordinating O^{2-} ligands that generate the crystal electric field are depicted as red spheres surrounding each of the four different Pr^{3+} ions shown as yellow spheres.

tering could in principle be used to determine these but that is beyond the scope of this paper. By analyzing the $T-$dependence of the magnetic susceptibility we can, however, obtain an estimate for the energy range associated with these crystal field levels. For this purpose, we fit the data to the following three component phenomenological form

$$\chi = \frac{C_0}{T} + 2k_B \sum_i \frac{C_i}{\Delta_i} \tanh \frac{\beta \Delta_i}{2}. \qquad (1)$$

Here $\beta = 1/k_B T$ and k_B is the Boltzmann constant. The first term is the Curie term, which we shall associate with Pr^{4+}impurities. The summations are over each of the four Pr^{3+} sites, which are approximated as two-level systems with a singlet ground state and excited levels at a characteristic energy Δ_i. This form is obtained as a low T approximation to the general Van Vleck susceptibility in the supplementary material (Eq.7)[46]. The expression has been constructed so that the high T limit takes the Curie-form C_i/T as for the impurity term. We found that two terms are sufficient to obtain excellent fits for all field directions.

The best fit parameters are listed in Table I. Consider first the fit to the poly-crystalline data. The sum of Curie constants $C_1 + C_2 = 1.63(2)$ (emu·K/Oe·mole) agrees well with the Curie constant for Pr^{3+} $C_{Pr^{3+}} = \mu_0 N_A g^2 J(J+1)\mu_B^2/(3k_B) = 1.60$ (emu·K/Oe·mole). The two polycrystal gap values provide a scale for the crystal field levels from 5 meV to 28 meV. For comparison the crystal field levels for $Pr_2Zr_2O_7$ are at [0, 10, 57, 82, 93, 109] meV[11]. The ratio of the Curie constants $C_1/C_2 = 0.77(1)$ indicates similar spectral weight at Δ_1 and Δ_2. The ratio $C_0/(C_1+C_2) = 0.53(1)\%$ provides the order of magnitude of the Kramers rare earth impurity concentration.

The fits to single crystal data yield a broader range of gap values with the smallest gap value $\Delta_1 = 3.93(7)$ meV associated with the easy (100) direction and the largest gap value $\Delta_2 = 50(1)$ meV for the (010) direction. The different energies Δ_i^α obtained for different field directions indicate the energy range for crystal field levels i with dominant contributions to the susceptibility for each field direction, α. However, with a total of 32 crystal field transitions available from the ground state of $Pr_2Ti_2O_7$, these data can only provide a general sense of the energy scale for the crystal field levels that contribute most to the Van Vleck susceptibility for each field direction. The Curie constants $C_i^{\alpha\alpha}$ for each field direction α reflect the site averaged dipolar matrix elements for crystal field levels separated by energies Δ_i^α for $i > 0$. The consistency between the directionally averaged single crystal parameters and those obtained for polycrystalline samples supports the evidence from x-ray diffraction that the single crystal and powder samples are similar at the atomic scale despite the very different growth conditions. We note the Curie constant associated with impurities $C_0^{\alpha\alpha}$ is more isotropic than for the intrinsic bulk terms $C_{1,2}^{\alpha\alpha}$. The impurity content as measured by C_0 is 40% less in the single crystal as compared to the powder samples.

In this insulating rare earth compound with shared ligands, super exchange interactions between praseodymium are expected to be on the 0.5 meV scale. This is an order of magnitude smaller than needed to close the lowest crystal field energy gap. The low-symmetry environment thus effectively renders the non-Kramers rare-earth ion compound non-magnetic and precludes a phase transition or indeed any truly collective physics. It might, however, be possible to induce a quantum phase transition through the application of pressure as in $TlCuCl_3$[70,71] and $Tb_2Ti_2O_7$[72] before inducing a structural phase transition.

B. Point charge model

The splitting of the $J-$multiplet and the associated magnetic single-ion anisotropy is due to the crystal electric field (CEF) associated with the ligands surrounding each rare earth ion. As detailed in the supplementary material[46], the corresponding single ion hamiltonian can

be expressed in the form

$$\mathcal{H}_{CEF} = \sum_{n,m} B_n^m O_n^m, \quad (2)$$

where O_n^m are Stevens operators[73,74] and B_n^m parametrize the effects of the CEF on the $J-$multiplet. Starting from the crystal structure, the point charge model yields estimates for B_n^m which are provided for each distinct Pr-site within $Pr_2Ti_2O_7$ in Table IV of the supplementary material[46].

Diagonalizing Eq. 2 yields the CEF level scheme shown for each of the four Pr Wyckoff sites in Fig. 6. The predicted contribution of crystal field level to the low T Van Vleck susceptibility for each of three field directions is listed in Table 5 of the supplementary material[46] and indicated by the color scheme in Fig. 6. The point charge model predicts that the Pr2 and Pr3 sites which are ten fold coordinated by oxygen and bracket the perovskite (001) slabs (Fig. 1), are the dominant contributors to the low T Van Vleck susceptibility (see also Fig. S1 of the supplementary material[46]).

The point charge model also indicates that the first excited CEF levels provide the largest contribution to the magnetic susceptibility. This support our use of the phenomenological form in Eq. 1 to fit the magnetic susceptibility data. Comparison of the point charge energy level scheme with that inferred from these fits shows a remarkable agreement in identifying the CEF levels that dominate the low T magnetic susceptibility for each of the three field directions. There is however, a consistent trend that the point charge model predicts lower energy levels than inferred from the phenomenological fitting. This is also apparent in Fig. 5(b) where the point charge model (dashed lines) generally overestimates the low T magnetic susceptibility. Overall though considering that there are no adjustable parameters, the point charge model does fairly well. For example it correctly predicts that $\chi^{a^*} > \chi^{b^*} > \chi^{c^*}$. Our analysis shows that Eq. 1 provides an excellent account of the anisotropic $T-$dependent magnetic susceptibility of this singlet ground state system. The corresponding energy levels on the far right in Fig.6 represent our best experimental estimate of the crystal field level scheme in $Pr_2Ti_2O_7$.

C. Curie tails and Pr^{4+} impurities

Examining the low field behavior in greater detail, Fig. 5(c) shows magnetization curves for various field directions at $T = 5$ K. For all orientations, the data look linear on this scale. However, if we subtract a linear fit to the high-field regime from 6.5 T to 7 T from the data, we obtain the non-linear component shown for the (001) direction in Fig. 5(d). Resembling the magnetization curve for a paramagnetic impurity, the non-linear component becomes more prominent when the thermal energy scale falls below the Zeeman energy scale. Under the assumption of a single characteristic impurity species it is possible to extract both the saturation magnetization and the impurity concentration from such data. To do so we fit the Langevin magnetization curve to the data

$$\Delta M(B,T) = f N_A \mu_{sat} L(\beta \mu_{sat} B). \quad (3)$$

Here f is the paramagnetic impurity fraction, N_A is Avagadro's number, and the Langevin function is given by $L(x) = \lim_{J\to\infty} B_J(x) = \coth(x) - 1/x$. $B_J(x)$ is the Brillouin function describing the magnetization curve for a paramagnetic impurity with spin-orbital angular momentum quantum number J. Fig. 5(d) shows that this functional form provides an excellent fit to the data with an impurity fraction of $f = 0.96(2)\%$ and a saturation moment of $\mu_{sat} = 2.00(3)\ \mu_B$. The Curie constant corresponding to these parameters is approximately $f\mu_0 N_A \mu_{sat}^2/(3k_B) = 0.0048(2)$ (emu·K/Oe·mole), which is entirely consistent with C_0 in Table I derived from T-dependent susceptibility data. Note that although the majority component of the magnetization is excluded from this analysis, the Langevin fit is consistent with the concentration estimate obtained from the ratio of Curie constants. We consider the concentration from the Langevin analysis to be more accurate though because it does not rely on the impurities having the same effective moment as the majority phase.

The specification of the Pr_6O_{11} starting material was $>$ 99% rare earth oxide with 99.99% of the rare earth oxide being Pr_6O_{11}. A non-Pr source for the paramagnetic impurity is thus unlikely. A possible explanation is that the rare earth impurity is Pr^{4+}, which has a single 4f electron and the same magnetic properties as Ce^{3+}. In particular it is a Kramers ion with a saturation moment of 2.14 μ_B, consistent with the Langevin analysis of the magnetization data.

V. CONCLUSION

We have successfully synthesized both polycrystalline samples and stoichiometric single crystals of $Pr_2Ti_2O_7$. Small levels of compositional deviations from the stoichiometric $Pr_2Ti_2O_7$ target compound lead to secondary phases of different, albeit related, structures. In contrast to the pyrochlore titanates, site disordering was not observed in the lower-symmetry monoclinic $Pr_2Ti_2O_7$ structure.

Building upon the chemical and structural stability of monoclinic $Pr_2Ti_2O_7$, we provide a process to grow large high-quality single crystals. Stoichiometric $Pr_2Ti_2O_7$ single crystals were grown for the first time using the traveling solvent floating zone (TSFZ) method. The susceptibility and magnetization measurements show no indications of a phase transition down to $T = 1.8$ K. Our analysis of the susceptibility data indicates a singlet ground state with excited CEF levels at energies ranging from 3.93(7) meV to 50(1) meV. This is as anticipated for the low-symmetry crystal electric field envi-

ronment associated with Pr^{3+} in monoclinic $Pr_2Ti_2O_7$. At sufficiently low density, Kramers rare earth impurities within $Pr_2Ti_2O_7$ behave as isolated paramagnetic impurities that dominate over the majority phase paramagnetic van-Vleck susceptibility at the lowest temperatures and fields ($T < 5$ K, $B < 5$ kOe). Analysis of the magnetization data in this regime yields a 0.96(2)% impurity content with a saturation moment of $\mu_{sat} = 2.00(3)\ \mu_B$, which is consistent with a low concentration of Pr^{4+} impurities.

The monoclinic structure contains a 3D network of Pr^{3+} with edge sharing ligand polyhedra assuring superexchange interactions on the 0.5 meV energy scale. If the gap between the two lowest lying singlets can be closed through the application of hydrostatic of uniaxial pressure, or fields, a quantum phase transition into an ordered magnetic state induced by these interactions can be anticipated. $Pr_2Ti_2O_7$ thus may provide an interesting opportunity to explore universal aspects of quantum critical spin dynamics in a material where large high quality crystals are attainable.

VI. ACKNOWLEDGEMENTS

This work was supported as part of the Institute for Quantum Matter, an Energy Frontier Research Center funded by the U.S. Department of Energy, Office of Science, Basic Energy Sciences under Award No. DE-SC0019331. H. Man, A. Ghasemi and C. L. Broholm were also supported by the Gordon and Betty Moore Foundation under GBMF9456. The work at University of Houston (M. Adnani and C. W. Chu) is supported by U. S. Air Force Office of Scientific Research Grants FA9550-15-1-0236 and FA9550-20-1-0068, the T. L. L. Temple Foundation, the John J. and Rebecca Moores Endowment, and the State of Texas through the Texas Center for Superconductivity at the University of Houston. Y. Li and C. L. Chien were supported by U.S. Department of Energy, Basic Energy Science under Award Grant No. DESC0009390. M. L. Taheri and E. Anber acknowledge funding in part from the US Department of Energy, Office of Basic Energy Sciences through contract DE-SC0020314. M. L. Taheri also acknowledges funding in part from the Office of Naval Research Multidisciplinary University Research Initiative (MURI) program through contract N00014-20-1-2368.

* koohpayeh@jhu.edu

[1] J. N. Millican, R. T. Macaluso, S. Nakatsuji, Y. Machida, Y. Maeno, and J. Y. Chan, Materials Research Bulletin **42**, 928 (2007).
[2] Y. Taguchi, Y. Oohara, H. Yoshizawa, N. Nagaosa, and Y. Tokura, Science **291**, 2573 (2001).
[3] M. A. Subramanian, B. H. Toby, A. P. Ramirez, W. J. Marshall, A. W. Sleight, and G. H. Kwei, Science **273**, 81 (1996).
[4] M. A. Subramanian, J. E. Greedan, and N. P. Raju, J. Phys. IV France **7**, 625 (1997).
[5] A. P. Ramirez and M. A. Subramanian, Science **277**, 546 (1997).
[6] M. Hanawa, Y. Muraoka, T. Tayama, T. Sakakibara, J. Yamaura, and Z. Hiroi, Phys. Rev. Lett. **87**, 187001 (2001).
[7] J. J. Ishikawa, E. C. T. O'Farrell, and S. Nakatsuji, Phys. Rev. B **85**, 245109 (2012).
[8] L. Balents, Nature **464**, 199 (2010).
[9] D. J. P. Morris, D. A. Tennant, S. A. Grigera, B. Klemke, C. Castelnovo, R. Moessner, C. Czternasty, M. Meissner, K. C. Rule, J.-U. Hoffmann, et al., Science **326**, 411 (2009).
[10] T. Fennell, P. P. Deen, A. R. Wildes, K. Schmalzl, D. Prabhakaran, A. T. Boothroyd, R. J. Aldus, D. F. McMorrow, and S. T. Bramwell, Science **326**, 415 (2009).
[11] K. Kimura, S. Nakatsuji, J. J. Wen, C. Broholm, M. B. Stone, E. Nishibori, and H. Sawa, Nat. Commun. **4**, 1934 (2013).
[12] R. Sibille, N. Gauthier, H. Yan, M. C. Hatnean, J. Ollivier, B. Winn, G. Balakrishnan, M. Kenzelmann, N. Shannon, and T. Fennell, Nature Phys. **14**, 711 (2018).
[13] T. A. Bojesen and S. Onoda, Phys. Rev. Lett. **119**, 227204 (2017).
[14] Y. Machida, S. Nakatsuji, S. Onoda, T. Tayama, and T. Sakakibara, Nature **463**, 210 (2010).
[15] B. Cheng, T. Ohtsuki, D. Chaudhuri, S. Nakatsuji, M. Lippmaa, and N. Armitage, Nat. Commun. **8**, 2097 (2017).
[16] K. A. Ross, L. Savary, B. D. Gaulin, and L. Balents, Phys. Rev. X **1**, 021002 (2011).
[17] S. Säubert, A. Scheie, C. Duvinage, J. Kindervater, S. Zhang, H. J. Changlani, G. Xu, S. M. Koohpayeh, O. Tchernyshyov, C. L. Broholm, et al., Phys. Rev. B **101**, 174434 (2020).
[18] A. Scheie, J. Kindervater, S. Zhang, H. J. Changlani, G. Sala, G. Ehlers, A. Heinemann, G. S. Tucker, S. M. Koohpayeh, and C. Broholm, Proceedings of the National Academy of Sciences **117**, 27245 (2020).
[19] M. Hirschberger, P. Czajka, S. M. Koohpayeh, W. Wang, and N. P. Ong (arXiv:1903.00595).
[20] A. Scheie, J. Kindervater, S. Säubert, C. Duvinage, C. Pfleiderer, H. J. Changlani, S. Zhang, L. Harriger, K. Arpino, S. M. Koohpayeh, et al., Phys. Rev. Lett. **119**, 127201 (2017).
[21] J.-J. Wen, S. M. Koohpayeh, K. A. Ross, B. A. Trump, T. M. McQueen, K. Kimura, S. Nakatsuji, Y. Qiu, D. M. Pajerowski, J. R. D. Copley, et al., Phys. Rev. Lett. **118**, 107206 (2017).
[22] J. S. Gardner, M. J. P. Gingras, and J. E. Greedan, Rev. Mod. Phys. **82**, 53 (2010).

[23] Y. Wang, T. Reeder, Y. Karaki, J. Kindervater, T. Halloran, N. Maliszewskyj, Y. Qiu, J. A. Rodriguez, S. Gladchenko, S. M. Koohpayeh, et al., Science Advances **7**, eabg0908 (2021).

[24] X. Zhang, Y. Luo, T. Halloran, J. Gaudet, H. Man, S. M. Koohpayeh, and N. P. Armitage, Phys. Rev. B **103**, L140403 (2021).

[25] A. Scheie, O. Benton, M. Taillefumier, L. D. C. Jaubert, G. Sala, N. Jalarvo, S. M. Koohpayeh, and N. Shannon (arXiv:2202.11085).

[26] L. Shcherbakova, L. Mamsurova, and G. Sukhanova, Russ. Chem. Rev. **48(3)**, 228 (1979).

[27] S. Kesari, N. P. Salke, S. J. Patwe, S. N. Achary, A. K. Sinha, P. U. Sastry, A. K. Tyagi, and R. Rao, Inorg. Chem. **55**, 11791-11800 (2016).

[28] P. Granger, V. Parvulescu, S. Kaliaguine, and W. Prellier, Perovskites and related mixed oxides (Chapter 11, pp. 233-257, 2016).

[29] L. Sun, L. Ju, H. Qin, M. Zhao, W. Su, and J. Hu, Physica B **431**, 49–53 (2013).

[30] A. Bayart, S. Saitzek, A. Ferri, R. Pouhet, M.-H. Chambrier, P. Roussel, and R. Desfeux, Thin Solid Films **553**, 71–75 (2014).

[31] S. J. Patwe, V. Katari, N. P. Salke, S. K. Deshpande, R. Rao, M. K. Gupta, R. Mittal, S. N. Achary, and A. K. Tyagi, J. Mater. Chem. C **3**, 4570 (2015).

[32] V. Atuchin, T. Gavrilova, J.-C. Grivel, V. Kesler, and I. Troitskaia, Journal of Solid State Chemistry **195**, 125–131 (2012).

[33] Z. P. Gao, H. X. Yan, H. P. Ning, and M. J. Reece, Advances in Applied Ceramics **112**, 69 (2013).

[34] S. Nanamatsu, M. Kimura, K. Doi, S. Matsushita, and N. Yamada, Ferroelectrics **8**, 511 (1974).

[35] H. Yan, H. Ning, Y. Kan, P. Wang, and M. Reece, J. Am. Ceram. Soc. **92**, 2270 (2009).

[36] M. N. Valdez and N. A. Spaldin, Polyhedron **171**, 181 (2019).

[37] N. Zakharov, V. Krikorov, E. Kustov, and S. Stefanovich, Phys. Status Solidi A **50**, K13 (1978).

[38] D. W. Hwang, J. S. Lee, W. Li, and S. H. Oh, J. Phys. Chem. B **107**, 4963 (2003).

[39] A. Sayede, R. Khenata, A. Chahed, and O. Benhelal, J. Appl. Phys. **113**, 173501 (2013).

[40] K. Krishnankutty and K. R. Dayas, Bulletin of Materials Science **31**, 907–918 (2008).

[41] S. Saha, S. Prusty, S. Singh, R. Suryanarayanan, A. Revcolevschi, and A. Sood, Journal of Solid State Chemistry **184**, 2204–2208 (2011).

[42] P. Kozmin, N. Zakharov, and M. Surazhskaya, Inorganic Materials **33**, 850 (1997).

[43] S. M. Koohpayeh, D. Fort, and J. S. Abell, Prog. Cryst. Growth Character. Mater. **54**, 121 (2008).

[44] S. M. Koohpayeh, Prog. Cryst. Growth Character. Mater. **62**, 22 (2016).

[45] G. M. Sheldrick, Acta Cryst. **C71**, 3 (2015).

[46] (See Supplemental Material at [] for solid state synthesis of polycrystalline samples, single crystal X-ray diffraction and the point charge model for the magnetic susceptibility).

[47] J. B. MacChesney and H. A. Sauer, Journal of The American Ceramic Society **45**, 416 (1962).

[48] S. D. Škapin, D. Kolar, and D. Suvorov, Journal of the European Ceramic Society **20**, 1179 (2000).

[49] Acta Crystallographica Section B: Structural Science, Crystal Engineering and Materials **69**, 249 (2013).

[50] G. M. Sheldrik, Acta Crystallographica Section A: Foundations of Crystallography **64**, 112 (2008).

[51] Y. Gong, R. Chu, Z. Xu, T. Dou, W. Zeng, X. Zhang, J. Hao, and G. Li, J. Am. Ceram. Soc. **99**, 2995 (2016).

[52] M. Kestigian and R. Ward, J. Am. Chem. Soc. **77**, 6199 (1955).

[53] S. Koohpayeh, J.-J. Wen, B. Trump, C. Broholm, and T. McQueen, Journal of Crystal Growth **402**, 291 (2014).

[54] A. Ghasemi, A. Scheie, J. Kindervater, and S. Koohpayeh, Journal of Crystal Growth **500**, 38 (2018).

[55] Q. Wang, A. Ghasemi, A. Scheie, and S. M. Koohpayeh, CrystEngComm **21**, 703 (2019).

[56] M. Yokoyama, T. Ota, I. Yamai, and J. Takahashi, J. of Crystal Growth **96**, 490 (1989).

[57] K. Yoshii, J. of Solid State Chemistry **149**, 354 (2000).

[58] F. Zhang, J. Lian, U. Becker, R. Ewing, L. Wang, J. Hu, and S. Saxena, J. of solid State Chemistry **180**, 571 (2007).

[59] R. D. Aughterson, G. R. Lumpkin, K. L. Smith, G. J. Thorogood, and K. R. Whittle, Mater. Res. Soc. Symp. Proc. **1107**, 365 (2008).

[60] R. D. Aughterson, G. R. Lumpkin, G. J. Thorogood, Z. Zhang, B. Gault, and J. M. Cairney, Journal of Solid State Chemistry **227**, 60 (2015).

[61] M. Abe and K. Uchino, Mat. Res. Bull. **9**, 147 (1974).

[62] K. E. Arpino, B. A. Trump, A. O. Scheie, T. M. McQueen, and S. M. Koohpayeh, Phys. Rev. B **95**, 094407 (2017).

[63] F. Bolz, Advanced Materials in Catalysis (Chapter 5, pp. 129-175, 1977).

[64] S. Hull, Rep. Prog. Phys. **67**, 1233–1314 (2004).

[65] T. Pussacq, H. Kabbour, S. Colis, H. Vezin, S. Saitzek, O. Gardoll, C. Tassel, H. Kageyama, C. L. Robert, and O. Mentré, Chem. Mater. **29(3)**, 1047 (2017).

[66] Rigaku Oxford Diffraction, CrysAlisPro Software System, Version 1.171, Rigaku Corporation **Oxford, UK** (2018).

[67] G. M. Sheldrik, University of Gottingen (2018).

[68] A. Scheie, Journal of Applied Crystallography **54**, 356 (2021).

[69] N. P. Salke, S. Kesari, S. J. Patwe, A. K. Tyagi, and R. Rao, AIP Conference Proceedings **1665**, 030011 (2015).

[70] C. Rüegg, A. Furrer, D. Sheptyakov, T. Strässle, K. W. Krämer, H.-U. Güdel, and L. Mélési, Phys. Rev. Lett. **93**, 257201 (2004).

[71] K. Goto, M. Fujisawa, T. Ono, H. Tanaka, and Y. Uwatoko, J. Phys. Soc. Jpn. **73**, 3254–3257 (2004).

[72] I. Mirebeau, I. N. Goncharenko, P. Cadavez-Peres, S. T. Bramwell, M. J. P. Gingras, and J. S. Gardner, Nature **420**, 54 (2002).

[73] M.T.Hutchings, Solid State Physics **16**, 227 (1964).

[74] K. Stevens, Proc. Phys. Soc. A **65**, 209 (1952).